DEFORMATION CHARACTERISTICS OF THE BUBBLE IN WATER-BIODIESEL IMMISCIBLE FLUIDS

by

Jiarui XU[a,b], Xiaohui ZHANG[a,b*], Shan QING[a,b], Hao ZHANG[a,b], and Hua WANG[a,b]

[a]Faculty of Metallurgical and Energy Engineering, Kunming University of Science and Technology, Kunming, China
[b]National Local Joint Engineering Research Center of Energy Saving and Environmental Protection Technology in Metallurgy and Chemical Engineering Industry, Kunming University of Science and Technology, Kunming, China

Original scientific paper
https://doi.org/10.2298/TSCI210724008X

It is of great significance to investigate the rising behavior of a bubble in immiscible fluids in chemical and metallurgical engineering. A 3-D model is established and the free-floating behavior of a single bubble in immiscible fluids (water-heavier liquid and biodiesel-lighter liquid) is numerically simulated by phase-field method. After the fluctuation of a certain distance, the bubble tends to be stable. It takes more time for the larger bubble to reach a stable shape than for the smaller one. The terminal aspect ratio of bubble, E_T, with the same size in heavier liquid is smaller than that in lighter liquid. With the increase of bubble size, E_T becomes small both in heavier and lighter liquid. Comparing bubble vortex diagrams of different shapes shows that the maximum vortex intensity is the direction in which the bubble shape extends. When the bubble passes through the liquid-liquid interface, it will form "pear", "inverted pear", "convex", and "water drop" shapes successively.

Key words*: single bubble, immiscible liquids, phase-field method, rising behavior*

Introduction

The gas-liquid multiphase flow is encountered in nuclear reactor [1], chemical [2], and metallurgical engineering [3]. Bubble motion characteristics are important in the gas-liquid flow, which closely relate to the heat and mass transfer and reaction rates. Bubble shape is a key factor of the motion characteristics. A lot of work had been carried out to study the bubble shape in a single liquid rather than immiscible liquids [4-7]. In many practical industrial processes [8], however, the bubble is in immiscible fluids.

The bubble deformation has often been evaluated by the aspect ratio, *E*, the ratio of the bubble minor axis to the major axis [4, 5]. Myint *et al.* [6] used distortion coefficient to describe the deformation of droplet, which was also used for the bubble deformation later.

*Corresponding author, e-mail: xiaohui6064@qq.com

Through theoretical analysis [9-11], experiments [12-15], and numerical simulations [16-18], the researchers proposed the relationship of E by taking into account all the forces on bubble, for example, the viscous, surface tension, buoyancy and inertial force. The forces on bubble are represented by dimensionless parameters Eotvos number (gravity *vs*. surface tension, Eo), Reynolds number (inertial force *vs*. viscous force, Re), Morton number (viscous force *vs*. surface tension, Mo). Grace *et al*. [19] drawn the regime diagram map of bubble shape related to dimensionless numbers Reynolds, Eotvos, and Morton. According to the regime diagram map, it was found that the shape of bubble was mainly determined by Reynolds and Eotvos numbers. Then the relationship between E and the dimensionless number was proposed. In a single liquid, researchers presented some empirical relations. The correlation proposed by Liu *et al*. [13] was applicable to the fluids with different viscosities, while Tomiyama's correlation [14, 15] was suitable for the fluids with different concentrations. In immiscible fluids, however, the deformation characteristics of bubble have not been reported. Bubble dynamics behavior is complex in immiscible liquids. Many scholars investigated the bubble motion behavior between the interface, such as rebound [20], coalescence [21], and flow regimes [21, 22] of the bubble. A few researchers studied the shape and velocity of a bubble in immiscible fluids. Grace *et al*. [19] analyzed the relationship between bubble velocity and shape and drawn regime diagram map. Mao *et al.* [23] carried out experiments, observed jet phenomenon of a single bubble at interface, and captured the changes of bubble shape, velocity and trajectory. Edrisi *et al.* [24] studied the effect of the bubble shape and rising pathway and proposed a novel procedure for the measurement of interfacial tension. Many studies on bubble shape in immiscible liquids were obtained by experimental methods. Compared with the experimental method, the numerical simulation has the advantages of safe operation and cost saving.

The phase-field method is widely used in multiphase flow, which is an interface capture method based on Cahn-Hilliard model [25]. There are many numerical simulation methods for multiphase flow, such as front tracking method [26], level set method [18], the volume-of-fluid [27], and some combined methods of these methods [28, 29]. Compared with these methods, the phase field method has the advantages of clear interface identification and surface tension model correction. The dynamic behaviour of the bubble is simulated by phase-field method in the immiscible fluids of water and biodiesel. The deformation characteristics of the bubble in immiscible fluids are studied. The relationship between steady shape and velocity of a bubble in the lower liquid and the upper liquid is obtained. The bubble instantaneous shape is closely related to vortex distribution. The formation of wake vortex causes the bubble to stay at interface for a longer time.

Model establishment and validation

Establishment of physical model

A 3-D model is established in fig. 1. Four different total fluid heights (30 mm, 50 mm, 75 mm, and 100 mm) are set, respectively. The width of the model is set to 10 times the diameter of the bubble to eliminate the wall effect [17]. The heights of the upper, H_1, and lower layers of liquid, H_2, are shown in fig. 2. and tab. 1, boundary conditions are shown in fig. 2. According to the density difference of the two fluids, they are divided into the lower liquid and the upper liquid, the physical properties are shown in tab. 2. The initial radius of the bubble is 2 mm, 2.5 mm, 3 mm, and 3.5 mm, respectively, and the initial height of bubble center is 5 mm.

Figure 1. Computational domain diagram

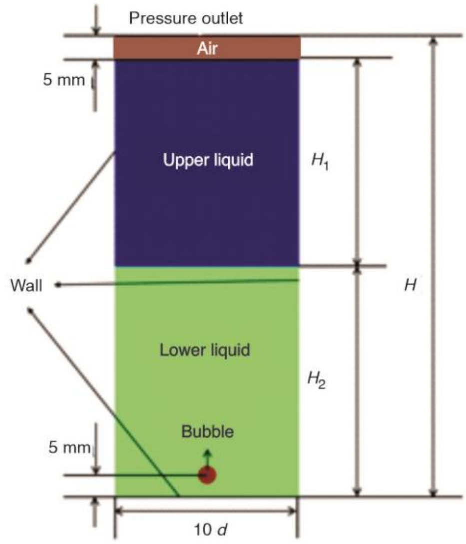

Figure 2. Schematic diagram of physical model

Table 1. Fluid heights of three group with different total heights

Total height of fluid, H [mm]	Height of lower fluid, H_2, [mm]	Height of upper fluid, H_1, [mm]
30	15	10
50	25	20
75	45	25
100	50	45

Table 2. Physical properties of materials

Fluid	Viscosity [Pas]	Density [kgm^{-3}]	Surface tension coefficient [Nm^{-1}]
Lower liquid	$1.003 \cdot 10^{-3}$	997.2	0.0727
air	$2.593 \cdot 10^{-5}$	1.205	–
Upper liquid	$4.6 \cdot 10^{-3}$	882.4	0.0321

Establishment of mathematical model

The fluid dynamics is calculated by the Navier-Stokes equation with surface tension force, as shown:

$$\rho\left(\frac{\partial u}{\partial t}+u\nabla u\right) = -\nabla p+\nabla\left[\eta\left(\nabla u+\nabla u^{t}\right)\right]+SF+\rho \mathrm{g} \tag{1}$$
$$\nabla u=0$$

where ρ [kgm^{-3}] is the density of the fluid, u [ms^{-1}] – the velocity of the fluid, p [Pa] – the pressure, η – the viscosity of the fluid, SF [N] – the surface tension of the interface, and g [ms^{-2}] – the gravitational acceleration.

The density and viscosity are constant in a single fluid, and the Navier-Stokes equation does not contain the surface tension term, but it is necessary to consider the surface tension between the interfaces of different fluids. The physical parameters at the interface of the three-phase flow follow the Gibbs triangle, *GT*, as shown:

$$GT = \left\{ \left(c_\mathrm{i}, c_\mathrm{j}, c_k \in \mathbb{R}^3 \right) \middle| \sum_{i=1}^{3} c_i = 1,\ 0 \le c_i \le 1 \right\} \tag{2}$$

where c_i, c_j, c_k represent a certain phase in the three-phase flow, which holds when $c_\mathrm{i} + c_\mathrm{j} + c_\mathrm{k} = 1$

The surface tension, *SF*, in the Navier-Stokes equation is given:

$$SF = -\sum_{\mathrm{i}=1}^{3} \alpha\varepsilon\gamma_i \nabla \cdot \left(\frac{\nabla c_i}{|\nabla c_i|} \right) |\nabla c_i| \nabla c_i \tag{3}$$

where γ_i represents the surface tension coefficient of the *i* fluid, $\sigma_\mathrm{ij} = \gamma_\mathrm{i} + \gamma_\mathrm{j}$ and σ_ij represents the surface tension coefficient between the *i* and *j* fluids.

Free energy is expressed by:

$$\Re = \int_{\Omega} \left[F\left(c_i, c_j, c_k\right) + \frac{\varepsilon^2}{2} \sum_{i=1}^{3} |\nabla c_i|^2 \right] \mathrm{d}x \tag{4}$$

where $F\left(c_\mathrm{i}, c_\mathrm{j}, c_\mathrm{k}\right) = 1/3\Sigma_{i=1}^{3} c_\mathrm{i}^2 \left(1 - c_\mathrm{i}\right)^2$ and Ω is an open, bounded subset of $\mathbb{R}^n$ (n = 1,2,3). The time dependence of c_i is given by the Cahn-Hilliard equation, the Cahn-Hilliard equation is shown in:

$$\frac{\partial c_i}{\partial t} + u c_i = \nabla\left(M \nabla \mu_i\right)$$

$$\mu_i = \frac{\partial F\left(c_i, c_j, c_k\right)}{\partial c_i} - \varepsilon^2 \Delta c_i + \beta\left(c_i, c_j, c_k\right) \tag{5}$$

$$S = \left(c_i, c_j, c_k\right) \equiv 1$$

$$\frac{\partial S}{\partial t} + u \nabla S = \nabla \left\{ M \nabla \left[\sum_{i=1}^{3} \frac{\partial F}{\partial c_i} - \varepsilon^2 \Delta S + 3\beta\left(c_i, c_j, c_k\right) \right] \right\} \tag{6}$$

where M is the migration, ε – the positive constant, and $\beta(c_\mathrm{i},c_\mathrm{j},c_\mathrm{k})$ – the non-constant Lagrange multiplier coefficient, and the sum of its variational derivatives is 0.

Grid independence verification

Figure 3 is a grid independence verification in the condition of 2 mm bubble radius with H = 100 mm, the cells are listed in tab. 3. As shown in fig. 3, with the increase of the maximum cell size, the bubble aspect ratio, E, decreases. Among the conditions for Grids A, B, C, D, Grid A has the highest accuracy, but the calculation cost is also highest. Considering the calculation cost and grid quality, Grid B is selected.

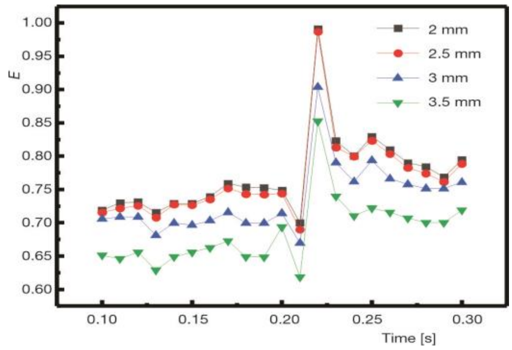

Figure 3. The *E* between liquid-liquid interface

Model validation

Mao *et al*. [23] studied the movement of bubbles with different sizes in water-oil immiscible fluids through experiments. In order to ensure the accuracy of present simulation, the experiment results of reference [23] are compared to the simulation results, which is

Table 3. Grid schemes investigation

	Maximum cell size [mm]	Number of nodes
Grid A	0.13	1272192
Grid B	0.15	954487
Grid C	0.18	665991
Grid D	0.20	534772

shown in fig. 4. The simulation conditions are set according to the experimental conditions of reference [23], tab. 4. The black and red points are the positions of the bubble at different times. The slope of line represents the velocity of the bubble. According to the comparison between the phase field model and the experimental results, therefore the phase-field model can be used to simulate bubble motion in immiscible fluids.

Table 4. Experimental conditions of reference [23]

	[23]	Simulation
The total height of the bubble movement [mm]	160	160
Initial bubble equivalent diameter [mm]	5.251	5.2
The height of the lower liquid [mm]	44	44

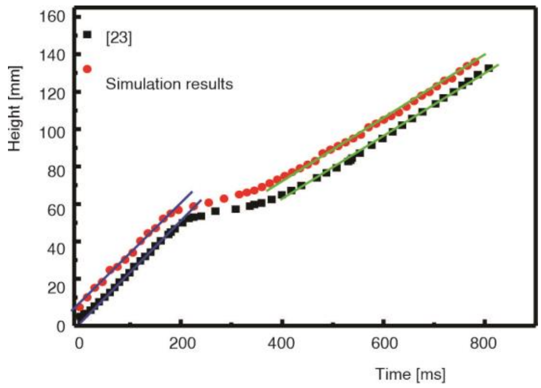

Figure 4. Comparison between the simulation results and reference [23]

Results and discussion

Bubble shape from lower liquid to upper liquid

In order to explore deformation characteristics of the bubble in lower fluid and upper fluid with different heights, four groups of different heights are set (in tab. 1). The bubble aspect ratio ($E = a/b$, in fig. 5) is used to characterize the shape change of the bubble [4, 5]. According to fig. 6, the change of E can be divided into four stages: Stage I – E decreases in the lower liquid, Stage II – E remains stable in the lower liquid, Stage III – E fluctuates up and down between the interface, and Stage IV – E remains stable in the upper liquid. Stage I and III occurred in four groups of heights, the four stages are obvious only when H = 100 mm, so the subsequent studies are based on H = 100 mm.

Figure 5. Schematic diagram of the typical bubble shape

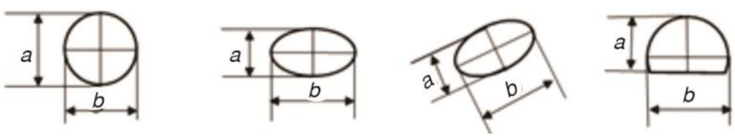

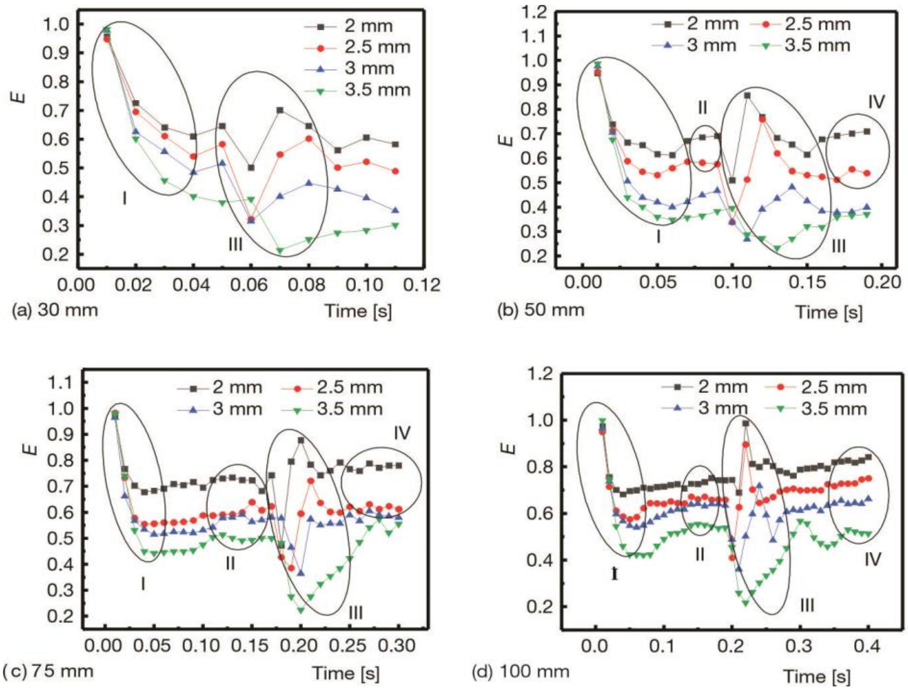

Figure 6. The change of *E* with time; (a) 30 mm, (b) 50 mm, (c) 75 mm, and (d) 100 mm

Figure 7 is the bubble velocity change with H = 100 mm. The bubble moves statically from the lower liquid to the upper liquid. The velocity change can be divided into six stages: Stage I – rises rapidly in the lower liquid, Stage II – drops in the lower liquid, Stage III – fluctuates up and down in the lower liquid, Stage IV – remains stable in the lower liquid, Stage V – fluctuates up and down between the interface, and Stage VI – remains stable in the upper liquid. When the bubble radius is small, there is no Stage II, that is, the velocity drops from the maximum value and then stabilizes. Through the comparison of bubble velocity and aspect ratio, it is found that the shape and velocity of the bubble in the upper liquid and the lower liquid remain stable.

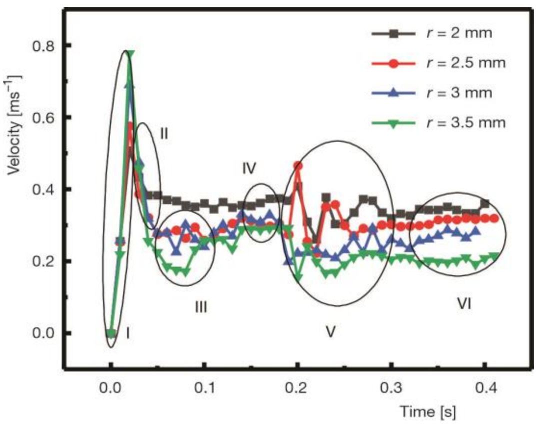

Figure 7. The velocity change with *H* = 100 mm

As shown in figs. 6(d) and 7, the bubble remains stable velocity and shape both in the lower liquid and the upper one after a certain distance, and the velocity and aspect ratio at this time are called the terminal velocity, V_T, and terminal aspect ratio, E_T. In fig. 8(a), with the increase of bubble radius, V_T decreases, V_T in the lower liquid is faster than in the upper liquid, and with the radius increase, the difference of V_T becomes larger. In fig. 8(b), with the increase of bubble radius, E_T decreases, E_T in the lower liquid is smaller than in the upper liquid, but with the radius increase, the difference of E_T becomes smaller. The reason is that the upper liquid has a larger viscous force. It is easier for the same size bubble to maintain a spherical shape with a larger viscous force. The smaller bubble is easier to maintain the spherical shape because of the greater surface tension on it, so the smaller bubble has a larger aspect ratio in upper liquid. Comparing figs. 8(a) and 8(b), it is not that the larger the bubble V_T, the larger the E_T.

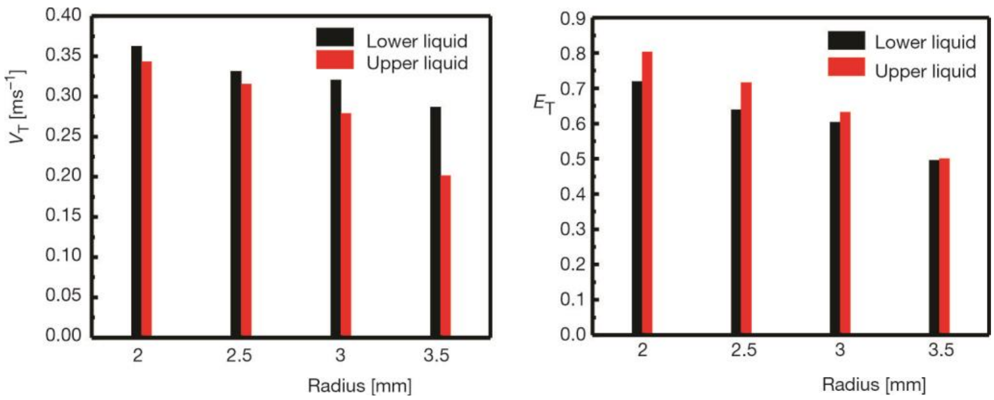

Figure 8. The V_T and E_T of different radius bubble; (a) V_T and (b) E_T

The bubble vortex distributions of different shapes are obtained, as shown in fig. 9. The strongest velocity vortex is marked with a red circle. When the bubble shape is approximately spherical, the maximum velocity vortex is distributed in the center of the bubble; When the bubble shape tends to be flat, the maximum velocity vortex is distributed on both sides of the bubble; When the bubble is convex, the maximum velocity vortex is distributed at the top of the bubble. The position of maximum velocity vortex distribution is the direction of bubble shape extension.

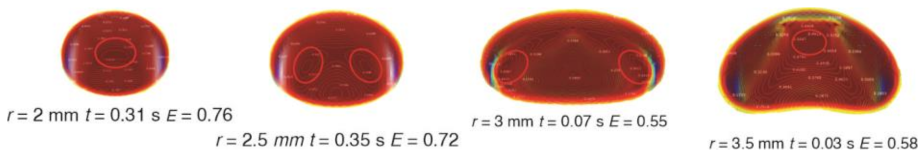

Figure 9. The bubble vortex distribution map in the lower liquid and upper liquid

Bubble shape between the interface

The shape of the bubble changes violently when it passes through the interface. To obtain the shape change of the bubble in the interface, E is taken every 0.001 seconds of movement when crossing the interface. Figure 10 shows the change of E when the bubble passes through the interface with H = 100 mm. In this process, E first decreases and then

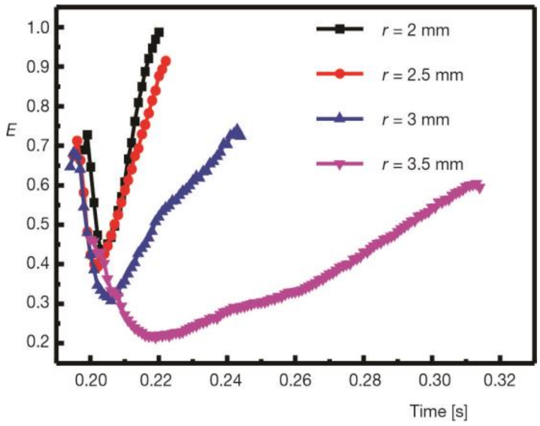

Figure 10. Changes of aspect ratio when crossing the interface

increases, and the decreasing time is shorter than increasing time, and with the increase of bubble size, the time difference becomes more obvious. It takes longer for E from small to large with the increase of bubble radius, because the wake vortex formed by the lower liquid at the bottom of the bubble inhibits bubble movement, and the larger the bubble is, the stronger the wake vortex is, fig. 11. The E is closer to 1 when the bubble is about to exit the interface than when it just contacts the interface. The reason is that the inertia force is weakened when the bubble just contacts the interface, and then the viscous force of the bubble is strengthened, but increases slowly.

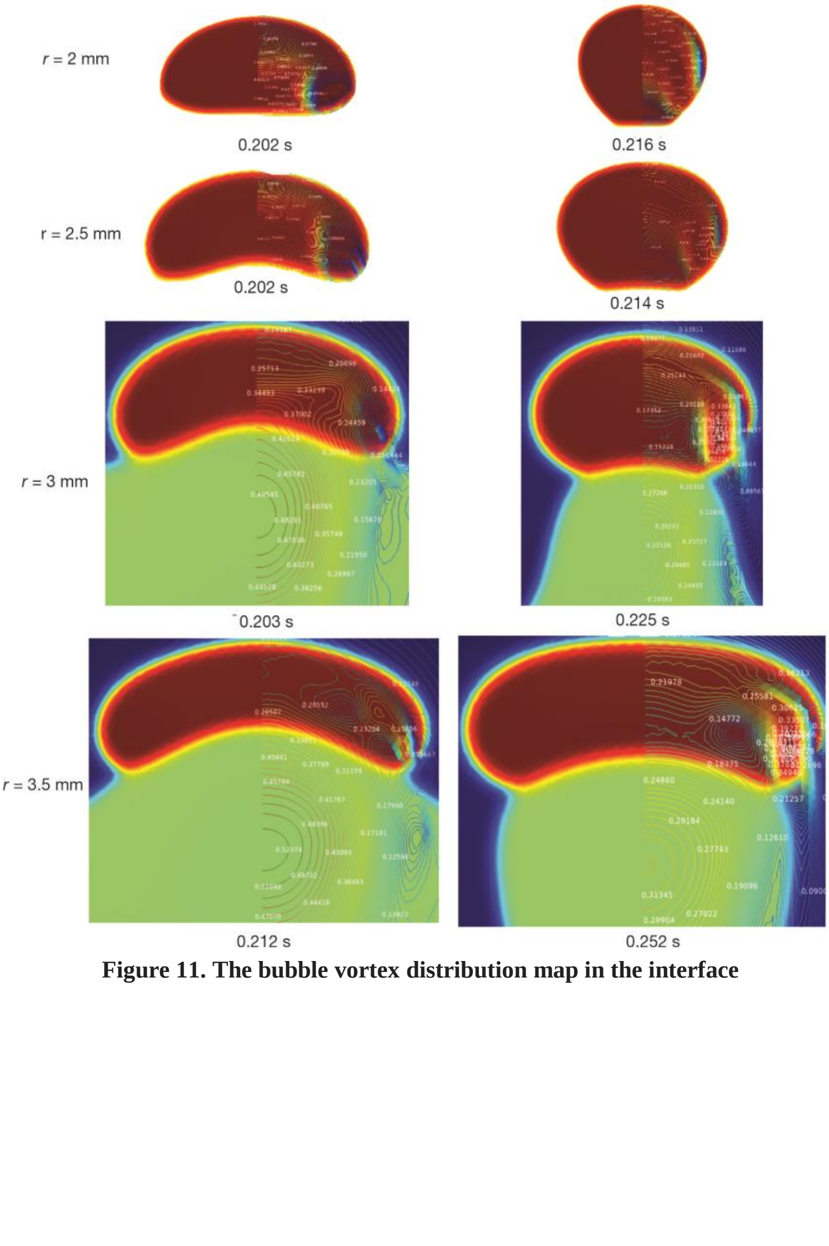

Figure 11. The bubble vortex distribution map in the interface

As shown in fig. 11, the vortex distribution map of the bubble passing through the interface is shown. According to fig. 10, E first decreases and then increases when the bubble crosses the interface, take a moment in the decreasing time period and increasing time period respectively, and then draw the vortex distribution, the red represents the bubble, the blue represents the lower liquid, the green represents the upper liquid and the solid line represents the velocity isoline. The bubble with a radius of 2 mm and 2.5 mm has obvious internal vortices. The bubble with a radius of 3 mm and 3.5 mm form a tail vortex, and the strength of the tail vortex increases as the bubble radius increases. The maximum wake vortex intensity of a bubble with a radius of 3 mm is 0.4954 m/s at 0.203 seconds, and a bubble with a radius of 3.5 mm is 0.5237 m/s at 0.212 seconds. The wake vortex causes the bubble to stay in the interface for a longer time.

By observing the profile of a bubble when passing through the liquid-liquid interface, it is found that when the bubble moves from touching the interface to leaving the interface, its shape is divided into the following four types in sequence: *pear* shape (a), inverted *pear* shape (b), *convex* shape (c), and *droplet* shape(d). The *pear* shape – E is close to 1, and the top of the bubble is narrower than the bottom. inverted *pear* shape – E is close to 1, and the top of the bubble is wider than the bottom. The *convex* shape – E is smaller, and the bubble is flat and convex. The *droplet* shape – E is close to 1, the bubble shape is nearly spherical and is generally a droplet shape. Figure 10 is the profile of a bubble with the radius of 2.5 mm.

Figure 12. The profile of the bubble when crossing interface (r = 2.5 mm)

Conclusions

The phase-field method is used to simulate the rising bubble in immiscible fluids. The shape changes of a bubble in water-biodiesel fluids are studied. In particular, four different shapes of the bubble at interface are observed and prediction method of the bubble transient shape is obtained. The conclusions are as follows.

- The bubble maintains stable shape and velocity in both heavier and lighter liquids with H = 100 mm. The E_T in the lower liquid is smaller than in the upper liquid. With the increase of radius, E_T in heavier liquid and lighter liquid becomes small. The V_T in the lower liquid is faster than in the upper liquid.
- The relationship between E_T and V_T. It is not that the larger the V_T, the larger the E_T. Comparing the instantaneous shape of the bubble with vortex distributions, it is found that the position of maximum velocity vortex distribution is the direction of bubble shape extension.
- When the bubble crosses the interface, the aspect ratio decreases rapidly and then slowly increases, and the aspect ratio is larger when it is about to leave the interface than when it just touches the interface. Moreover, the larger the bubble is, the longer the bubble crosses the interface.
- Between the interface, the bottom of the larger bubble (r = 3 mm, 3.5 mm) will form a tail vortex, and as the bubble radius increases, the strength of the tail vortex increases. The wake vortex causes the bubble to stay in the interface for a longer time.

- There are four shapes of bubble when it crosses the interface: *pear* shape, *inverted pear* shape, *convex* shape, and *water drop* shape. The change from *pear* shape to *inverted pear* shape is short-lived, and the period of maintaining convex shape is longer.

Acknowledgement

The research is supported by National Natural Science Foundation of China (No. 51966005) and Yunnan Fundamental Research Projects (No. 202101AT070120).

Nomenclature

a	– bubble width [mm]
b	– bubble height [mm]
c	– order parameter [–]
E	– aspect ratio [–]
E_T	– terminal aspect ratio [–]
g	– gravitational acceleration [ms^{-2}]
GT	– Gibbs triangle [–]
H	– fluid height [mm]
M	– mobility coefficient [m]
p	– pressure [Pa]
r	– bubble radius [mm]
SF	– surface tension of the interface [N]
t	– time [s]
u	– fluid velocity [ms^{-1}]
V_T	– bubble terminal velocity [ms^{-1}]

Greek symbols

β	– lagrange multiplier [–]
ε	– interfacial width [m]
η	– viscosity [Pa·s]
ρ	– density [kgm^{-3}]
σ	– surface tension coefficient [Nm^{-1}]

Subscripts

1,2	– upper liquid and lower liquid
i, j, k	– fluid phase

References

[1] Saraswat, S. P., *et al*., Linear Stability Analysis of RELAP5 Two-Fluid Model in Nuclear Reactor Safety Results, *Ann. Nucl. Energy, 149* (2020), 107720
[2] Kalmar, C., *et al.*, Relationship Between the Radial Dynamics and the Chemical Production of a Harmonically Driven Spherical Bubble, *Ultrason. Sonochem., 64* (2020), 104989
[3] Hallet, V., *et al*., The Impact of Slag Fineness on the Reactivity of Blended Cements with High-Volume Non-Ferrous Metallurgy Slag, *Constr. Build. Mater., 257* (2020), 119400
[4] Tomiyama, A., Drag, Lift and Virtual Mass Forces Acting on a Single Bubble, *Procedings*, International Symposium on Two-Phase Flow Modelling and Experimentation, Pisa, Italy, 2004
[5] Rastello, M., Lance, *et al*., Drag and Lift Forces on Clean Spherical and Ellipsoidal Bubbles in a Solid-Body Rotating Flow, *J. Fluid. Mech., 682* (2011), July, pp. 434-459
[6] Myint, W., *et al*., Shapes of Single Drops Rising Through Stagnant Liquids, *J. Fluid. Sci. Tech., 2* (2007), 1, pp. 184-195.
[7] Hallmark, B., *et al*., Experimental and Simulation Studies of the Shape and Motion of an Air Bubble Contained in a Highly Viscous Liquid Flowing Through an Orifice Constriction, *Chem. Eng. Sci., 206* (2019), 6, pp. 272-288
[8] Wang, Q., *et al.*, Multiphase Equilibrium Modeling of Oxygen Bottom-Blown Copper Smelting Process, *Trans. Nonferrous Met. Soc. China, 27* (2017), 11, pp. 2503-2511
[9] Rayleigh, L., *et al*., On the Pressure Developed in a Liquid During the Collapse of a Spherical Cavity, *Philos. Mag., 34* (1917), 200, pp. 94-98
[10] Milton, S., *et al*., Collapse of an Initially Spherical Vapour Cavity in the Neighbourhood of a Solid Boundary, *J. Fluid Mech., 47* (1971), 2, pp. 283-290
[11] Plesset, M. S., *et al*., Bubble Dynamics and Cavitation, *Annu. Rev. Fluid. Mech., 9* (1977), Plessed, pp. 145-185
[12] Tian, Z., *et al*., Bubble Shape and Rising Velocity in Viscous Liquids at High Temperature and Pressure, *Exp. Therm Fluid Sci., 102* (2019), Apr., pp. 528-538
[13] Liu, L., *et al*., Experimental Studies on the Shape and Motion of Air Bubbles in Viscous Liquids, *Exp. Therm Fluid Sci., 62* (2015), Apr., pp. 109-121
[14] Aoyama, S., *et al*., Shapes of Ellipsoidal Bubbles in Infinite Stagnant Liquids, *Int. J. Multiphase. Flow., 79* (2016), Mar., pp. 23-30

[15] Aoyama, S., *et al*., Shapes of Single Bubbles in Infinite Stagnant Liquids Contaminated with Surfactant. *Exp. Therm. Fluid Sci., 96* (2018), Sept., pp. 460-469
[16] Yan, P., CFD Simulation of Hydrodynamics in a High-Pressure Bubble Column using Three Optimized Drag Models of Bubble Swarm, *Chem. Eng. Sci., 199* (2019), 4, pp. 137-155
[17] Xu, Y., *et al*., Numerical Investigations on Bubble Behavior at a Steel-Slag Interface, *Steel Res. Int., 91* (2020), 6, pp. 1-7
[18] Balcazar, N., *et al*., Level-Set Simulations of Buoyancy-Driven Motion of Single and Multiple Bubbles, *Int. J. Heat Fluid Flow, 56* (2015), Dec., pp. 91-107
[19] Grace, J. R., *et al*., Shapes and Velocities of Single Drops and Bubbles Moving Freely Through Immiscible Liquids, *Trans. Inst. Chem. Eng., 54* (1976), 3, pp. 167-173
[20] Singh, K. K., *et al*., Bouncing of a Bubble at a Liquid-Liquid Interface, *AIChE J.,63* (2017), 7, pp. 3150-3157
[21] Emery, T. S., *et al*., Flow Regimes and Transition Criteria during Passage of Bubbles through a Liquid-Liquid Interface, *Langmuir, 34* (2018), 23, pp. 6766-6776
[22] Bonhomme, R., *et al*., Inertial Dynamics of Air Bubbles Crossing a Horizontal Fluid-Fluid Interface, *J. Fluid Mech.,707* (2012), Sept., pp. 405-443
[23] Mao, N., *et al*., Formation and Detachment of the Enclosing Water Film as a Bubble Passes through the Water-Oil Interface, *Colloids Surf., A, 202* (2020), 11, 124236
[24] Edrisi, A., *et al*., A Novel Experimental Procedure to Measure Interfacial Tension Based on Dynamic Behavior of Rising Bubble through Interface of Two Immiscible Liquids, *Chem. Eng. Sci., 231* (2021), 116255
[25] Kim, J., Phase Field Computations for Ternary Fluid Flows, *Comput. Method. Appl. M., 196* (2007), 45-48, pp. 4779-4788
[26] Hua, J., *et al*., A Front Tracking Method for Simulation of Two-Phase Interfacial Flows on Adaptive Unstructured Meshes for Complex Geometries, *Int. J. Multiphase Flow.,119* (2019), Julz, pp. 166-179
[27] Hirt, C. W., *et al*., Volume of Fluid (VOF) Method for the Dynamics of Free Boundaries, *J. Comput. Phys., 39* (1981), 1, pp. 201-225
[28] Sun, D. L., *et al*., A Coupled Volume-of-Fluid and Level Set (VOSET) Method for Computing Incompressible Two-Phase Flows, *Int. J. Heat Mass Transf., 53* (2010), 4, pp. 645-655
[29] Chakraborty, I., A Coupled Level-Set and Volume-of-Fluid Method for the Buoyant Rise of Gas Bubbles in Liquids, *Int. J. Heat Mass Transf., 58* (2013), 1, pp. 240-259

Paper submitted: July 24, 2021
Paper revised: January 2, 2022
Paper accepted: January 3, 2022